Twenty-Seventh Symposium (International) on Combustion/The Combustion Institute, 1998/pp. 1497–1505

COMPUTATIONAL AND EXPERIMENTAL STUDY OF SOOT FORMATION IN A COFLOW, LAMINAR ETHYLENE DIFFUSION FLAME

C. S. McENALLY,[1] A. M. SCHAFFER,[1] M. B. LONG,[1] L. D. PFEFFERLE,[1] M. D. SMOOKE,[1] M. B. COLKET[2] AND R. J. HALL[2]

[1]*Yale Center for Combustion Studies*
Yale University
New Haven, CT 06520-8284, USA
[2]*United Technologies Research Center*
East Hartford, CT 06108, USA

A sooting, ethylene coflow diffusion flame has been studied both experimentally and computationally. The fuel is diluted with nitrogen and the flame is slightly lifted to minimize the effects of the burner. Both probe (thermocouple and gas-sampling techniques) and optical diagnostic methods (Rayleigh scattering and laser-induced incandescence) are used to measure the temperature, gas species, and soot volume fractions. A detailed soot growth model in which the equations for particle production are coupled to the flow and gaseous species conservation equations has been used to investigate soot formation in the flame. The two-dimensional system couples detailed transport and finite-rate chemistry in the gas phase with the aerosol equations in the sectional representation. The formulation includes detailed treatment of the transport, inception, surface growth, oxidation, and coalescence of soot particulates. Effects of thermal radiation and particle scrubbing of gas-phase growth and oxidation species are also included. Predictions and measurements of temperature, soot volume fractions, and selected species are compared over a range of heights and as a function of radius. The formation of benzene is primarily controlled by the recombination of propargyl radicals, and benzene production rates are found to limit the rate of inception as well as the net rate of soot growth. The model predicted soot volume fractions well along the wings of the flame but underpredicted soot volume fractions by a factor of four along the centerline. Oxidation of particulates is dominated by reactions with hydroxyl radicals that attain levels approximately ten times higher than calculated equilibrium levels. Gas cooling effects due to radiative loss are shown to have a very significant effect on predicted temperatures.

Introduction

Combustion-generated soot particulates from land-based sources pose a significant health risk and are the subject of stringent new EPA regulations. Now, soot emissions from aircraft face the likelihood of tightened regulation. Besides regulatory issues, soot contributes to thermal radiation loads on combustor liners and turbine blades. Soot emissions enhance contrail formation and tactical visibility of military aircraft. Further, impaction of soot on low observable surfaces can compromise the radar signature of aircraft. Quantitative understanding of the soot growth and oxidation mechanisms and the ability to model accurately these processes may be critical to the development of strategies to control emissions.

Despite the complexities of modeling soot formation in flames using detailed chemistry, the linkage of soot production to radiation and bulk flame properties is so strong that the coupled treatment of this problem is becoming a necessity for quantitative modeling of flame structure. Such modeling for a generic multidimensional configuration is still beyond our current computational ability. The laminar diffusion flame, however, provides an environment to investigate the interaction of soot formation with detailed gas-phase chemistry in a multidimensional system.

Recent investigators [1,2] have modeled jet diffusion flames, using simplified, monodisperse soot formation models with skeletal kinetic mechanisms. We recently modified the sectional soot formation model developed in Refs. [3,4] for incorporation into a code for a laminar axisymmetric diffusion flame (cylindrical fuel jet surrounded by a coflowing oxidizer) [5]. This model employs a velocity-vorticity formulation [6] in which the governing conservation equations are solved with detailed transport and finite-rate chemistry submodels to predict the temperature, species mass fractions, and velocity fields as functions of the two independent coordinates. When this model was applied to a sooting methane–air flame, comparisons between the model and experiments were reasonable, yet the matching of bulk

flame properties was insufficient to enable quantitative comparison of the calculated and measured soot profiles. In contrast to these results was the nearly perfect agreement obtained between the model and optical diagnostics of temperature, fuel, and NO for a nonsooting, methane coflow diffusion flame [7]. This latter blue flame was diluted and lifted far from the burner inlet. A speculated problem in the sooting flame that was attached to the burner was uncertain inlet boundary conditions due to preheating of the fuel and air.

This investigation studies a coflow diffusion flame, but partially lifted, to minimize effects of uncertain inlet conditions and to compare results from calculations, intrusive diagnostics, and nonintrusive diagnostics to determine the strengths and weaknesses of each approach. Through this study, it is expected that flame types amenable to modeling, and correspondingly appropriate diagnostic methods, can be recommended for future studies. Furthermore, this study should provide additional information on the nature of soot formation and growth in coflow diffusion flames.

Problem Formulation

Soot Modeling

Soot kinetics are modeled as coalescing, solid carbon spheroids undergoing surface growth in the free molecule limit. The particle mass range of interest is divided into sections [8], and an equation is written for each section including coalescence, surface growth, and oxidation. Sectional analysis makes it possible to obtain the particle size distribution without *a priori* assumptions about the form of the distribution. For the smallest section, an inception source term is included. The transport conservation equation for each section includes thermophoresis, an effective bin diffusion rate, and source terms for gas-phase scrubbing. The gas and soot equations are additionally coupled through nonadiabatic radiative loss in the optically thin approximation. The inception model employed here is based on an estimate of the formation rate of two- and three-ringed aromatic species (naphthalene and phenanthrene) and is a function of local acetylene, benzene, phenyl, and molecular hydrogen concentrations [5]. The contributions from the inception processes are incorporated in the first sectional bin, whose lower mass boundary is set equal to the mass of the smallest inception species. In the sectional representation [8], the sectional mass boundaries vary linearly on a logarithmic scale. The number of sections required for convergence must be examined for each problem and depends on the relative magnitudes of surface growth and inception. Oxidation of soot by O_2 and OH is treated as described in [4]. The surface growth rate is based on that of Harris and Weiner [9] with a nominal activation energy of 31.8 kcal/mol as suggested by Hura and Glassman [10]. We empirically adjusted the Harris and Weiner rate by a factor of two as in Ref. [5].

Governing Equations and Numerical Method

The axisymmetric computational model employs the gas-phase diffusion flame equations in the velocity-vorticity formulation [6] with the sectional approach presented in Ref. [4]. Buoyancy is included in the model. The result is a strongly coupled set of elliptic partial differential equations. We solve for the radial and axial velocities, the vorticity, the temperature, the gas-phase species, and the particle sectional mass fractions. The system is closed with the ideal gas law, and appropriate boundary conditions are applied on each side of the computational domain. Local properties are evaluated using vectorized and highly optimized transport and chemistry libraries [11]. The sectional thermophoretic velocities in the free molecule regime are given in Ref. [3] as are the sectional diffusion velocities, which are written with a mass-weighted mean diffusion coefficient for each size class. In the optically thin radiation model used in our calculations, the significant radiating species, in addition to particulates, are H_2O, CO, and CO_2. Given the length scales of the flame investigated, it is highly unlikely that self-absorption is important. Although the soot volume fraction reaches near ppm levels, the narrowness of the soot shell (1–2 mm) will mitigate any self-absorption effects.

The governing conservation equations are solved on a two-dimensional mesh by combining a steady-state and a time-dependent solution method [7]. A time-dependent approach is used to help obtain a converged numerical solution on an initial coarse grid. Grid points are then inserted adaptively, and Newton's method is used to complete the problem.

Experimental Methods

Atmospheric pressure, overventilated, axisymmetric, coflowing, non-premixed laminar flames were generated with a burner in which the fuel flows from an uncooled 4.0-mm-i.d. vertical brass tube (wall thickness 0.038 mm) and the oxidizer flows from the annular region between this tube and a 50-mm diameter concentric tube (see Fig. 1). The oxidizer was air while the fuel was a mixture containing ethylene and nitrogen. Fuel flowrates were governed by electronic mass flow controllers accurate to within 5%. The same burner apparatus was used for all the experiments. The temperature of the brass tube for this slightly lifted flame was less than 330 K.

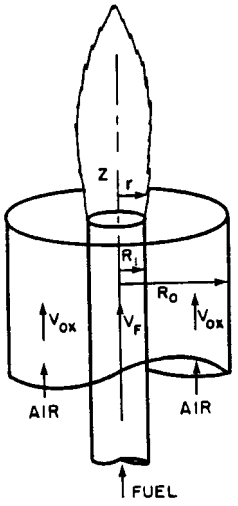

FIG. 1. Schematic of the burner configuration.

Probe Measurements

The probe measurement procedures have been described previously [12,13]. Gas temperatures were measured with 75 μm wire-diameter Type R thermocouples and corrected for radiation heat transfer effects using standard techniques [12]. A rapid insertion procedure was used to minimize errors due to soot deposition onto the thermocouple. In soot-free regions, the absolute uncertainty of these measurements is estimated to be ± 50 K and the relative uncertainty to be ± 10 K.

Soot concentrations were measured with the same thermocouples using thermocouple particle densitometry (TPD), a technique in which soot volume fraction is inferred from measured rates of soot particle mass transfer to the thermocouple junction [12]. The results have a relative uncertainty of 30%, and an absolute uncertainty of 50%.

Species concentrations were measured by extracting gas samples from the flames with a narrow-tipped quartz microprobe and analyzing these samples with on-line mass spectrometry [13]. Acetylene and ethylene were quantified with an Extrel C50 variable-ionization-energy electron-impact/quadrupole mass spectrometer, and C3 to C12 hydrocarbons with a custom-built photoionization/time-of-flight mass spectrometer. Measurements were directly calibrated and have an absolute uncertainty of 30%.

Profiles were generated by moving the burner with translation stages. The axial and radial coordinates, designated z and r, have a relative uncertainty of ± 0.2 mm and an absolute uncertainty of ± 0.5 mm.

Laser Diagnostic Measurements

Using planar laser imaging, we obtain two-dimensional fields of temperature, fuel concentration, and soot volume fraction in the C_2H_4/N_2 flame. The temperature field is determined using the two scalar approach of Stårner et al. [14] and included the measurement of Rayleigh scattering and the use of the computed fuel concentration.

The soot volume fraction field is determined by laser-induced incandescence (LII). At sufficient laser intensities, the LII signal has been shown to be directly proportional to soot volume fraction [15]. The probe measurements of the soot volume fraction are used for calibration.

The second harmonic of an Nd:YAG laser (532 nm) is focused into a 18.0-mm-tall vertical sheet over the center of the burner. The incandescence and scattered light is collected perpendicular to the laser axis. The light passes through an appropriate interference filter and then is focused onto an intensified charge-coupled device (CCD) camera.

For Rayleigh scattering, images at two downstream locations are acquired. For the first set of images, the laser sheet is 3 mm off the surface of the burner. A 532-nm interference filter (10-nm FWHM) is used to collect the Rayleigh scattering. In the region from 11.0–22.0 mm downstream, interference from LII and particle scattering dominate the Rayleigh signal, which is not plotted in this region (see Fig. 2). Rayleigh images are also acquired with the bottom edge of the laser sheet just above the flame tip (22 mm off the burner surface), where temperatures are just below adiabatic flame temperatures, and where there is no interferences from LII. Laser energy is set to 100 mJ/pulse.

With the laser sheet 8 mm off the burner surface, LII images are acquired. A 450-nm (10-nm FWHM) interference filter is used to collect the incandescence signal. In the region of greatest incandescence signal, a survey is conducted of incandescence signal versus laser intensity to maximize signal intensity without saturation (e.g., soot destruction) at any point in the flowfield. All images are corrected for optical throughput, background scattering signals, and nonuniformities in beam profile. Images are also corrected for flame luminosity and nonuniform detector response.

Results

The chemical kinetic mechanism for ethylene combustion has 45 species and 233 reactions. It was derived from GRIMech 1.2 [16], based on comparisons to experimental data on ethylene from perfectly stirred and flow reactors and ignition delay data. It includes reactions describing the formation and oxidation of benzene, and related species.

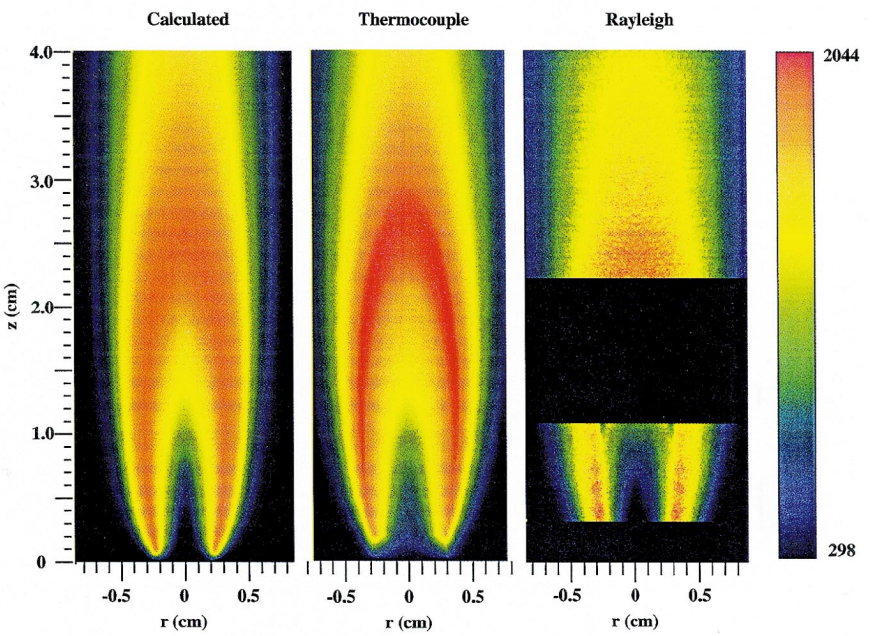

FIG. 2. Temperature isotherms (K) for the model (left), thermocouple (center), and Rayleigh scattering (right) measurements.

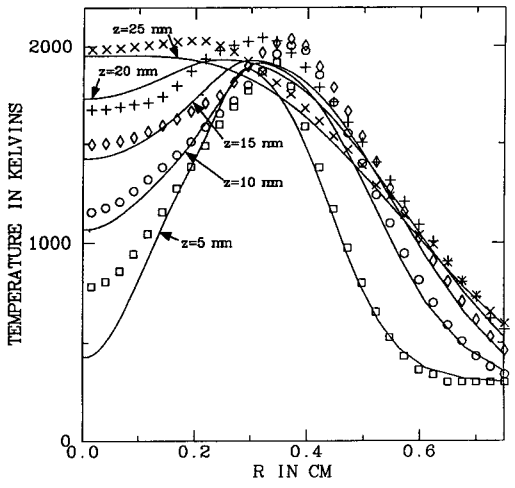

FIG. 3. Comparison between the experimental thermocouple temperature measurements and the computed temperatures as a function of the radial coordinate at several axial heights (□ = 5 mm, ○ = 10 mm, ◇ = 15 mm, + = 20 mm, × = 25 mm).

Fuel and nitrogen are introduced through the center tube (4-mm i.d.) utilizing a parabolic velocity profile and air through the outer coflow with a plug flow profile. Both velocity profiles were those employed in the experiments. The mass fractions at the burner exit are 0.32 and 0.68 for ethylene and nitrogen, respectively, and the bulk averaged velocity is 35 cm/s. The coflow air velocity was 35 cm/s. Reactant temperatures were assumed to be 298 K. All radial velocities were assigned to zero at the flame base.

Calculations were performed on an IBM RS/6000 Model 590 computer. In the computations presented, nine soot size classes were included in the model with approximately 10,000 adaptively refined grid points. Starting from a converged solution for an ethylene–air flame without the sectional equations, we typically obtained converged solutions for the complete gas-soot problem in several hours of computer time. The number of soot bins in these calculations was constrained by the maximum memory of our computer. Based on the relative magnitudes of the inception and surface growth rates, we anticipate that the restricted number of bins has not caused significant numerical error.

In Fig. 2, temperatures determined from the model, the thermocouple, and Rayleigh scattering are compared. Radial comparisons between the computations and thermocouple measurements at

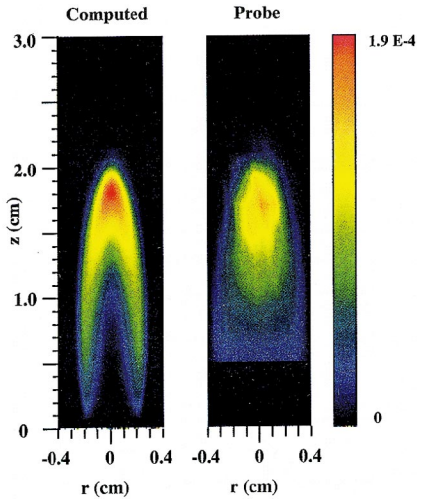

FIG. 4. Comparison between the computed and experimental benzene mole fraction isopleths.

several axial locations are plotted in Fig. 3. Agreement between the temperature computations and measurements is excellent throughout the flame. The peak temperatures were 1953 K for the computations and 2040 K for the thermocouple measurements. Peak Rayleigh temperatures were somewhat lower than the computations. With radiation from soot suppressed, the peak predicted temperature is 1990 K; with both gas band and soot radiation suppressed, the peak predicted temperature rises to 2061 K. Integration of the computed radiative dissipation over the flame volume yields a predicted radiative power that is about 12% of the total heat release. Flame height, as estimated by the attainment of the peak temperature on the centerline was 2.7 ($\pm$0.05) cm for all three cases. This agreement is dramatically better than that obtained in the attached methane–air diffusion flame [5] in which the experimental inlet conditions were not well defined. It also should be noted that the excellent agreement on the air side of the flame contrasts with the results obtained in [5] where there was substantial difference between the measured and computed temperatures. The calculated rise in temperature along the centerline is delayed relative to the increase as determined from the probe measurements, but it is in good agreement with the optical results. We speculate that accurate determination of temperatures in this region of the flame, where thermal gradients are very large, with a thermocouple is difficult due to conduction along the thermocouple wires.

Ethylene profiles were obtained from all three methods; two-dimensional contour plots and the radial profiles at various axial heights (not shown here) depict excellent agreement among the model and the Raman scattering experiments. Peak concentrations of acetylene, the principal carbon-containing species involved in surface growth, as calculated by the model and as determined by the probe measurements are 4.3% and 3.7%. Peak concentrations are located along the centerline about 15 mm above the burner lip, and generally the profile shapes agree well, at least in regions of the flame that do not have other contributions to the mass 26 peak. Experimentally, acetylene decays a little faster along the centerline than does the model. Contours for benzene are shown in Fig. 4. Peak predicted benzene mole fractions are 1.8×10^{-4} versus a peak experimental value of 1.6×10^{-4}. A reaction path analysis demonstrated that benzene was formed principally through propargyl recombination reactions (to form $H + C_6H_5$). Propargyl, in turn, is formed through the oxidation of diacetylene, that is, $C_4H_2 + OH \rightarrow C_3H_2 + HCO$ followed by C_3H_2 recombination with H-atoms. When soot inception scrubbing of benzene is not activated in the model, the peak benzene concentration increases by a factor of 38%. This contrast demonstrates the importance of scrubbing effects and demonstrates how benzene levels are determined based on a balance of its formation and its conversion to higher molecular weight hydrocarbon species. Other than the inception process, the principal loss mechanism for benzene in these fuel-rich, pyrolytic zones is via the thermal decomposition of phenyl radical, and such decomposition does not occur rapidly until the gas temperature exceeds 1800 K, a point after the bulk of soot inception and growth has occurred.

Soot volume fractions f_v, as determined from the model, thermophoretic sampling, and LII (calibrated based on probe measurements) are illustrated in Fig. 5. Agreement between the two experimental techniques is considered very good. Peak soot f_v from the model agrees well with the experimental values; however, soot still peaks off the centerline in the wing region for the model and on the centerline for the two sets of experiments. Peak values are 7.85×10^{-7} for the model and 1.0×10^{-6} for the thermophoretic measurements. When the predicted values ultimately peak along the centerline, they are a factor of four below the measured value. As illustrated, the thermophoretic sampling method detects soot particles closer to the burner than does LII. The sampling method has the ability to detect not only carbonized soot but any translucent particles as well. We also note in Fig. 5 that the computations illustrate an extended wing region compared with that of both experimental methods. This is due, in part, to the fact that the soot volume fraction in the lower wing regions are below the lower detectivity limits of the experimental methods. In Fig. 6 we compare computational and thermophoretic sampling soot volume fractions as a function of the radial coordinate at several axial heights.

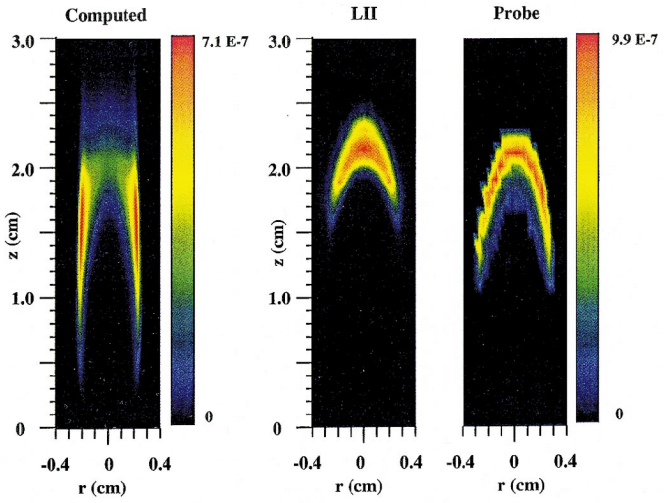

FIG. 5. Comparison of computed (left) and experimental soot volume fraction isopleths. The right picture contains the thermophoretic sampling measurements. The center figure contains the laser-induced incandescence measurements.

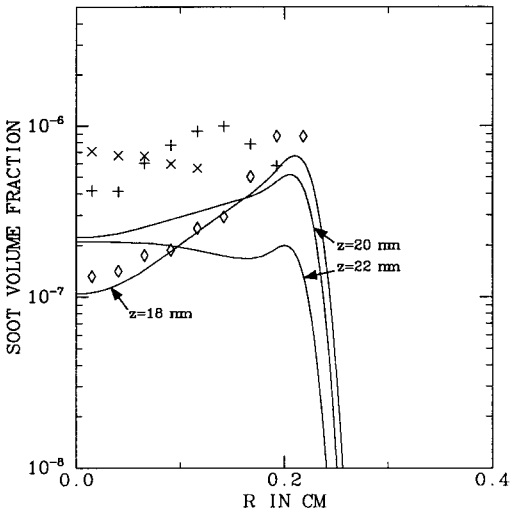

FIG. 6. Comparison between the computed and experimental (thermophoretic sampling technique) soot volume fraction as a function of the radial coordinate at several axial heights ($\diamond$ = 18 mm, + = 20 mm, $\times$ = 22 mm).

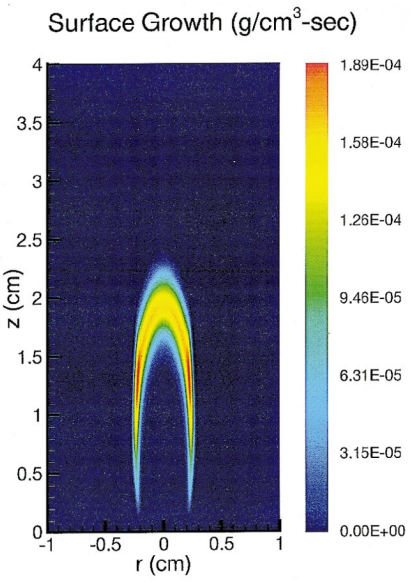

FIG. 7. Computed soot surface growth isopleths for the ethylene diffusion flame.

Although the agreement at 18 mm is excellent, it is clear that the model does fall short in being able to predict soot values that are as large as those measured on the centerline. The tendency for soot to peak in the wings is typically observed in more heavily sooting flames [2]. Relative spatial distributions for the separate processes of surface growth, soot inception, and oxidation as determined from the model are illustrated in Figs. 7, 8, and 9, respectively.

A brief analysis of these results indicates that the high soot oxidation rates observable in the wings of this flame are attributable to superequilibrium OH concentrations, consistent with our previous study [5] and that of several previous investigations [17]. The lack of including the effects of superequilibrium OH in such coflow flames are likely to result in significant errors in the analysis/interpretations. Variations in the base soot model surface growth, inception, and oxidation rates were carried out to gain understanding of the possible causes of the difference between the model and the experiments. These studies did not yield a clean explanation of the discrepancies. We conclude that the ability to make

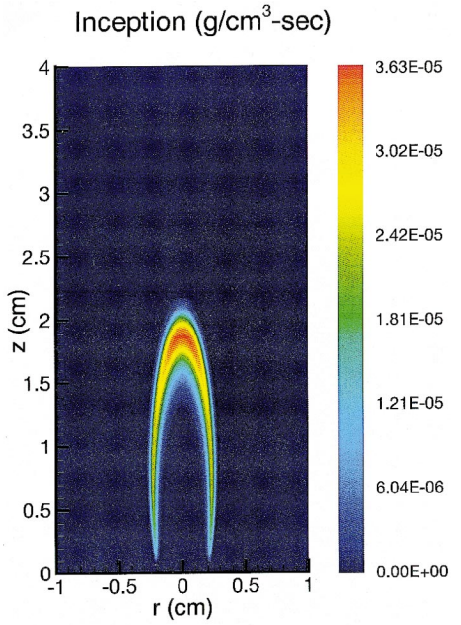

FIG. 8. Computed soot inception isopleths for the ethylene diffusion flame.

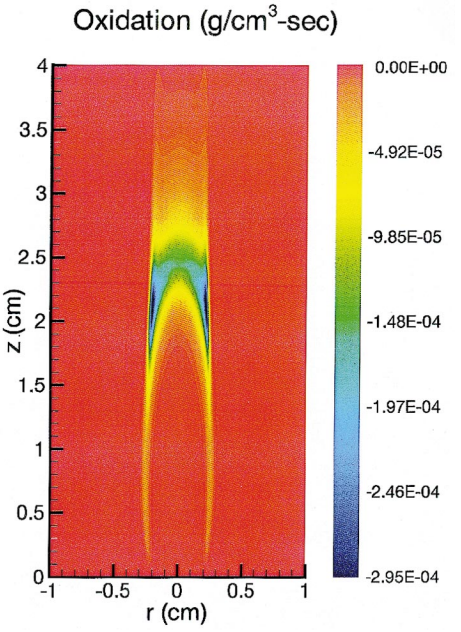

FIG. 9. Computed soot oxidation ($OH + O_2$) isopleths for the ethylene diffusion flame.

quantitative soot predictions remains limited by some fundamental uncertainties in the soot model (including the lack of aging and aggregate formation effects), by the ability of the chemical kinetic mechanism to predict accurately the concentrations of important species (benzene, propargyl, acetylene, and diacetylene) and possibly by the lack of quantitative information concerning the production of translucent particles [18].

Conclusions

A slightly lifted ethylene jet diffusion flame was investigated by comparing results from two sets of experimental diagnostics, one of which was intrusive and the other nonintrusive, and results from a detailed model with fully coupled equations treating radiation and soot formation. The current work is the first to apply a detailed chemistry model with a multiple section soot growth model to a flame that has well represented burner/inlet conditions. Agreement among the experiments and computations is generally good and in some cases excellent. In addition, by comparing the results, we were able to conclude that previously identified discrepancies [5] were likely the result of uncertainties in the burner inlet conditions when the flame is attached to the burner lip. Specifically, uncertain inlet conditions previously led to overprediction of the flame height and high temperatures in the wings of the flame. For the lifted flame, the model was able to reproduce bulk flame parameters extremely well, including flame height, species concentrations, and local temperatures, given some uncertainties in the experiments. The coupled soot model utilized in this and in previous studies reproduced peak soot volume fractions to within 20% but had some difficulty in reproducing accurately the distribution of soot formed along the centerline of the flame versus that formed along the wings. The formation of benzene as a limit to the inception process was confirmed in this study. Benzene formation was found to be governed by propargyl recombination, and propargyl formation, in turn, was controlled by reactions involving diacetylene.

Acknowledgments

This work has been supported in part by the Air Force Office of Scientific Research under contract F49620-94-C-0059 and the United States Department of Energy, Office of Basic Energy Sciences. The encouragement of Julian Tishkoff and discussions with R. J. Santoro (Penn State University), R. A. Dobbins (Brown University), and M. A. Tanoff (Yale University) are gratefully acknowledged. The assistance of B. A. Bennett and B. Dobbins (Yale University) was essential in the preparation of the figures.

REFERENCES

1. Kaplan, C. R., Shaddix, C. R., and Smyth, K. C., *Combust. Flame* 106:392–405 (1996).
2. Kennedy, I. M., Rapp, D. R., Santoro, R. J., and Yam, C., *Combust. Flame* 107:368–382 (1996).
3. Colket, M. B. and Hall, R. J., in *Soot Formation in Combustion, Mechanisms and Models* (H. Bockhorn, ed.), Springer Series in Chemical Physics 59, Springer-Verlag, New York, 1994, pp. 442–470.
4. Hall, R. J., Smooke, M. D., and Colket, M. B., in *Physical and Chemical Aspects of Combustion: A Tribute to Irvin Glassman* (R. F. Sawyer and F. L. Dryer, eds.), Combustion Science and Technology Book Series, Gordon & Breach, Langhorne, PA, 1997, pp. 189–230.
5. Smooke, M. D., McEnally, C. S., Pfefferle, L. D., Hall, R. J., and Colket, M. B., "Computational and Experimental Study of Soot Formation in a Coflow, Laminar Diffusion Flame," *Combust. Flame,* in press (1997).
6. Ern, A., Douglas, C. C., and Smooke, M. D., *Int. J. of Supercomputer Appl.* 9:167–186 (1995).
7. Smooke, M. D., Ern, A., Tanoff, M. A., Valdati, B. A., Mohammed, R. K., Marran, D. F., and Long, M. B., in *Twenty-Sixth Symposium (International) on Combustion,* The Combustion Institute, Pittsburgh, 1996, pp. 2161–2170.
8. Gelbard, F. and Seinfeld, J. H., *J. Coll. Int. Sci.* 78:485–501 (1980).
9. Harris, S. J. and Weiner, A. M., *Combust. Sci. Technol.* 31:155–167 (1983).
10. Hura, H. S. and Glassman, I., in *Twenty-Second Symposium (International) on Combustion,* The Combustion Institute, Pittsburgh, 1988, pp. 371–378.
11. Giovangigli, V. and Darabiha, N., in *Proceedings of the Conference on Mathematical Modeling in Combustion,* Lyon, France, NATO ASI Series, 1987, pp. 491–503.
12. McEnally, C. S., Köylü, Ü. Ö., Pfefferle, L. D., and Rosner, D. E., *Combust. Flame* 109:701–720 (1997).
13. McEnally, C. S. and Pfefferle, L. D., *Combust. Sci. Technol.* 116–117:183–209 (1996).
14. Stårner, S., Bilger, R. W., Dibble, R. W., and Barlow, R. S., *Combust. Sci. Technol.* 86:223–236 (1992).
15. Quay, B., Lee, T.-W., Ni, T., and Santoro, R. J., *Combust. Flame* 97:384–392 (1994).
16. Bowman, C. T., Hanson, R. K., Davidson, D. F., Gardiner, W. C. Jr., Lissianski, V., Smith, G. P., Golden, D. M., Frenklach, M., Wang, H., and Goldenberg, M., *GRI-Mech version 2.11,* http://www.gri.org (1995).
17. Puri, R., Santoro, R. J., and Smyth, K. C., *Combust. Flame* 97:125–144 (1994).
18. Dobbins, R. A., Fletcher, R. A., and Lu, W., *Combust. Flame* 100:301–309 (1995).

COMMENTS

Houston Miller, George Washington University, USA. As I understand your presentation, "soot" was considered as a series of increasing size bits, the smallest of which was a two-ring aromatic. Clearly, experimental diagnostics such as the thermophoretic thermocouple technique are not measuring species as small as these. I wonder what the comparisons between model and experiments would look like had the definition of the minimum paper size been increased to a more realistic value.

Author's Reply. The TPD technique will detect any particle massive enough to condense onto the thermocouple (roughly above 1000 amu). Based on an analysis of predicted particle size distributions for this ethylene flame and for a methane flame (Fig. 11 in Ref. [5] in the paper), the contributions of the low mass classes (1–3) to the total soot field are insignificant on locations where soot concentrations are at measurable levels. Because particles with masses below 1000 amu all fall within the first size class for the present study, our figures and conclusions will not be effected. Separating these classes will be useful, however, for investigation whether our model simulates experimental results on PAH species. Such comparisons have not yet been performed.

•

Carolyn Kaplan, Naval Research Laboratory, USA. Your results indicate that soot nucleation peaks at the centerline and that surface growth is high at the centerline. Can you suggest a reason as to why the computed soot volume fraction is so low at the centerline? Could it be that the computed oxidation is too high? Also, can you tell (from the computations) what the gas-phase temperature is at particle inception?

Author's Reply. We have tried to determine the cause of the low soot predictions along the centerline using a preliminary sensitivity analysis on the effects of variable oxidation rates, growth rates, and inception rates, presumably due to the relative spatial location of peak values for these rates (Figs. 7–9 in the paper). Our best estimate is that the deficit in the model is caused by inaccuracies in our PAH growth/inception model. Based on a comparison of particle inception rates and gas-phase temperatures, predicted inception rates begin to increase dramatically in the 1550–1650 K regime, consistent with arguments presented by Glassman [1].

REFERENCE

1. Glassman, I., in *Twenty-Seventh Symposium (International) on Combustion,* The Combustion Institute, Pittsburgh, 1998, pp. 1589–1596.

•

Richard Wainner, Georgia Tech, USA. A number of modeling efforts and some experimental results have shown the LII signal to be sensitive to particle size, especially at longer delays from the laser pulse. As your particle sizes are known (and extend over a broad range), you might want to correct your LII signal for this spatially varying sensitivity and then see how well this profile compares with the thermocouple deposition data.

Author's Reply. The experimental volume fraction profiles obtained by LII and thermocouple deposition are in good overall agreement. However, the qualitative shape of the computed soot volume fraction shows some significant differences—most notably the computed soot volume fraction profiles do not peak on the centerline. Therefore, even though the computations do include information on the size distribution, we do not feel confident in using computed particle sizes to correct the measured LII profiles.